J. Electrochem. Sci. Eng. **14(6)** (2024) 705-717; http://dx.doi.org/10.5599/jese.2439

Open Access : : ISSN 1847-9286
www.jESE-online.org

Original scientific paper

Effect of CoO loading on electrochemical properties of activated carbon from sugarcane bagasse

Kyfti Yolanda Siburian[1], Al Nadine De Nasti[1], Enjeli Rotama Sidauruk[1], Haryo Satriya Oktaviano[2], Nona Merry M. Mitan[3], Lisna Efiyanti[4], Nur Adi Saputra[4], Nur Layli Amanah[1] and Agung Nugroho[1,✉]

[1]*Department of Chemical Engineering, Faculty of Industrial Technology, Universitas Pertamina, Jakarta, Indonesia*
[2]*Research and Technology Innovation, PT Pertamina (Persero), Jakarta, Indonesia*
[3]*Department of Chemistry, Faculty of Science and Computer, Universitas Pertamina, Jakarta, Indonesia*
[4]*Research Center for Biomass and Bioproduct, National Research and Innovation Agency, Jl. Raya Bogor KM 46, Bogor 16911, Indonesia*

Corresponding author: ✉ *agung.n@universitaspertamina.ac.id; Tel.: +62-822-99649611*

Received: July 23, 2024; Accepted: November 4, 2024; Published: December 10, 2024

Abstract

Activated carbon is synthesized from sugarcane bagasse (SB) through a pre-carbonization process in a muffle furnace at 400 °C, followed by carbonization and activation using the pyrolysis method at 800 °C. In the activation process, pre-carbonized SB is activated using 0.1 M NaOH. The activated carbon is then impregnated with cobalt oxide (CoO) using a hydrothermal method at 110 °C to improve its electrochemical performance. After impregnation, the presence of CoO is confirmed by X-ray diffraction patterns. Scanning electron microscopy suggests that the samples' morphology shows pore structures. Electrochemical properties are measured by cyclic voltammetry and galvanostatic charging-discharging techniques using a three-electrode system with 1 M Na_2SO_4 as an electrolyte. It is found that the specific capacitance of activated carbon from SB is 89.53 F/g, while after impregnation with CoO, it increases to 102.04 F/g at the same current density of 0.05 A/g.

Keywords

Biomass; sugar industry byproduct; activated carbon production; cobalt oxide impregnation; specific capacitance

Introduction

Along with population growth that increases every year, there is an increase in energy demand that seriously affects the environment. Therefore, some alternative storage devices that are environmentally friendly are highly needed to overcome energy problems and global warming. In

recent years, the transition to alternatives has become the focus of researchers to realize energy storage devices that are cheap, have large capacities, and can be used for a long time. Such energy storage devices are batteries, capacitors, or those that involve hydrogen, magnetic, and pump energy storage [1].

In this context, supercapacitors are part of a promising technology for preserving electrical energy because of their advantages, such as a large power density, long life cycle, and good reversibility properties. Aside from those advantages, supercapacitors have potential applications in hybrid vehicles, electronic devices, and renewable energy-based smart grid management. Today, supercapacitors act as energy storage devices that bridge gaps such as cell voltage and specific power between batteries and conventional capacitors. Supercapacitors differ from ordinary conventional capacitors//batteries in their ability to store energy. Supercapacitors are energy storage devices that can be charged almost instantly and release energy over time. Also, they can be charged multiple times with minimal degradation in performance. Although having a fast charge-discharge, the supercapacitor's energy density is low due to the limited charge time due to the surface of the electrode material used. This makes it necessary to increase the specific capacitance and potential window, which is done by choosing electrode materials with high capacitance. One of the electrodes commonly used to improve the performance of supercapacitors is made from carbon-based materials [2-4].

Activated carbon (AC) is a porous carbon material with a large specific surface area and is applied in various fields, such as adsorption and catalysis, where it produces high-value products. AC can be obtained from biomass, usually composed of three main components: cellulose, hemicellulose, and lignin. Materials with a greater lignin content will produce AC with a macroporous structure, while materials with higher cellulose content will produce AC with a predominantly microporous structure [5,6]. Sugarcane bagasse (SB) is one of the biomasses that has the potential because bagasse waste has a cellulose content of 43.6 %, lignin of 18.1 % and hemicellulose of 33.5 % [7].

To improve capacitive properties, AC has been frequently applied in the form of composites with transition metal oxides, which, by fast redox reaction, contribute to pseudocapacitive properties of electrode material. The synthesized metal oxides, including NiO, ZnO, Mn_2O_3, and $CuCo_2O_4$, are frequently utilized as electrode materials for pseudocapacitors due to their high theoretical capacitance [8]. However, one of the main challenges is their relatively short cycle life. To address this issue, one approach is to convert the material into a nanostructure. This modification can increase the active surface area and stability of the material, thus improving the cycle life and overall performance of the pseudocapacitor [9,10]. However, it has low performance on high current rate density.

Among transition metal oxides, cobalt (II) oxide (CoO) has been selected because of its high conductivity, which promotes efficient electron transfer and ensures consistent redox reactions. Furthermore, CoO exhibits outstanding electrochemical activity, leading to high specific capacitance and effective energy storage. Its fast and reversible redox reaction capacity makes it an ideal choice for applications requiring rapid energy storage and release [11,12]. Therefore, CoO is quite interesting for further investigations. It has been declared a promising electrode for supercapacitors due to its low-cost environmental footprint and high theoretical capacitance (3560 F/g). CoO shows good electrical conductivity and the ability to store the charge of ions during the electrochemical process, which would affect the electrochemical performance of the supercapacitor [13].

In this study, SB is pre-carbonized, activated using chemical activation, and impregnated by different amounts of the synthesized CoO. Thus, obtained SB-based samples are tested for their surface and electrochemical properties.

Experimental

Materials

SB was obtained from one of the sugarcane drink stalls in Jakarta, washed with water to remove impurities, and then dried in an oven at 110 °C for 12 hours to remove water content. NaOH used for SB activation was obtained from Merck CAS-No: 1310-73-2. $CoSO_4 \cdot 7H_2O$ from PT Smart LAB Indonesia CAS: 10026-24-1 was used as a precursor for preparing CoO, while Na_2SO_4 for electrolyte is obtained from Fischer Chemical CAS: 7757-82-6.

Experimental methods

The synthesis of AC from SB was carried out using three main processes: pre-carbonization by pyrolysis method, chemical activation using NaOH, and impregnation with cobalt oxide using the hydrothermal method. Chemical activation is preferred over physical activation because it can achieve greater yields at lower temperatures, create distinct pore structures and shorten reaction times [14].

Preparation of activated carbon

Dried SB samples were mashed and filtered using a 100-mesh sieve. In the pre-carbonization process, 5.6 g of SB was transferred into a crucible and put into a furnace at 400 °C for 2 hours to produce pyrochar. This sample was defined as LAT-Pre. After pre-carbonization, 1 g of pyrochar was activated with 0.1 M NaOH solution and stirred for 2 hours. Then, the sample was filtered, put into crucibles for carbonization and entered in a tube furnace at 800 °C for 1 hour in an Ar gas flow. After carbonization, the AC sample was cooled to room temperature and washed with deionized (DDI) water until pH was close to neutral. The washed sample was dried in a vacuum oven at 70 °C for 8 h. This sample was defined as LAT-AC.

Synthesis of cobalt oxide

Cobalt(II) oxide (CoO) was synthesized by preparing 1 M solution of $CoSO_4 \cdot 7H_2O$ by dissolving 281.14 g of $CoSO_4 \cdot 7H_2O$ in 1 L of deionized water (DDI) and stirring the mixture for 20 minutes. After that, 40 mL of 2 M NaOH solution was poured slowly into 40 mL of prepared $CoSO_4 \cdot 7H_2O$ solution and stirred for 30 minutes until it produced a blue precipitate. Then, the solution was filtered and dried at 100 °C for 4 hours and calcined at 300 °C for 1 hour to produce CoO.

Impregnation of cobalt oxide into activated carbon

The impregnation of CoO into AC was carried out by the hydrothermal method. A solution was prepared by mixing 0.1 g of AC in 120 mL of DDI water, subsequent addition of CoO (0.1, 0.05 and 0.025 g) (sequentially called LAT-AC-CoO-1; LAT-AC-CoO-05; LAT-AC-CoO-025) into the solution, and stirring for 30 minutes. Then, the final solution was put into a 200 mL Teflon-lined hydrothermal autoclave and heated in an oven at 110ºC for 6 hours. After the hydrothermal process, the AC/CoO material was filtered and washed until neutral pH was attained, and then it was finally dried in a vacuum oven at 70 °C for 8 hours.

Characterizations

The functional groups of the prepared SB-based samples were analyzed using FTIR Thermo Scientific iS 5 with a 500 to 4000 cm^{-1} wavelength range. Raman analysis was used to accurately determine the degree of carbonization. XRD was used to characterize the crystal structure of the samples at a diffraction pattern of 10 to 80° with a PANalytical instrument with CuKα radiation. The morphological structure of the sample surfaces was characterized using SEM (accelerated voltage of

20 kV) with magnifications of 10000×. Meanwhile, EDX was used to analyze the elements composition in each sample.

Working electrode preparation

The working electrode, *i.e.,* the modified glassy carbon electrode, was prepared using the drop-casting method. First, a cast ink was prepared by mixing 1.6 mg of each sample (LAT-PRE, LAT-AC and LAT-AC-CoO) with 0.5 mL of isopropanol in a glass vial. The mixture was sonicated for 30 minutes to ensure homogeneity. Separately, the glassy carbon electrode was sonicated for 30 minutes, dried, and polished using specialized sandpaper from Metrohm to clean its surface. Subsequently, 6 µL of the prepared ink was drop-cast onto the cleaned glassy carbon with an area of 7.065 mm^2 using a micropipette. After drying, 3 µL of Nafion solution was drop-cast onto the surface.

Electrochemical measurements

For the electrochemical testing, Ag/AgCl was used as the reference electrode, which served as a stable reference point for measuring the potential of the working electrode. A Pt wire was used as the counter electrode to facilitate the current flow necessary for the electrochemical reaction to occur on the glassy carbon as the working electrode where the redox reaction occurs. These three electrodes were assembled in a three-electrode system within a beaker containing 1 M Na_2SO_4 as the electrolyte [15].

Results and discussion

Table 1 presents the chemical compositions of all prepared SB-based (LAT-Pre, LAT-AC and LAT-AC-CoO) samples and the carbon yield after SB treatment using the pre-carbonization method, chemical activation, and impregnation steps. The LAT-Pre sample is a sample before the activation process, while LAT-AC is a sample obtained after the activation process using NaOH. The carbon yield obtained from the LAT-Pre sample is only 34.2 %. The low yield is due to heat treatment at 400 °C, which causes the decomposition of chemical components within the temperature range of 240 to 400 °C [16,17]. The yield calculation considers only the carbon content without including the weight of the activators such as NaOH or CoO. This approach leads to a lower reported yield percentage since the contribution of additional compounds used in the activation process is excluded.

Table 1. *Carbon yield for SB samples after pre-carbonization, activation and impregnation*

Sample	Composition (AC : CoO weight ratio)	Yield, %
LAT-Pre	-	34.2
LAT-AC	-	10.5
LAT-AC-CoO-025	1 : 0.25	1.7
LAT-AC-CoO-05	1 : 0.5	1.7
LAT-AC-CoO-1	1 : 1	1.9

After activation, the yield drastically decreases to 10.5 %, as presented in Table 1. The decomposition of the acid group causes a low yield after activation at a temperature range of 100 to 650 °C. After the activation process, the carbon formed has only organic functional groups [18]. After CoO addition, a further decrease in carbon yield from the previous AC sample is observed. The low carbon yield after CoO addition could be due to the water and gas content from raw materials. After the hydrothermal process was completed, the sample experienced a significant decrease in mass because of the release of water and gas content.

Based on the FTIR results shown in Figure 1(a), SB samples have O-H functional groups in the range of 3334 cm^{-1} before pre-carbonization. In addition, there are functional groups C-H, C=C, C=O

and C-O. The presence of functional groups on the LAT-Pre sample shows that this sample has the potential to activate carbon [19]. All carbon functional groups disappeared during the activation and impregnation process. The high-temperature condition at 800 °C causes the sample to decompose and makes the organic structure of SB split. Additionally, after the impregnation process, the FTIR test results in a peak in the range of 559 cm^{-1}, which indicates a peak of CoO [20].

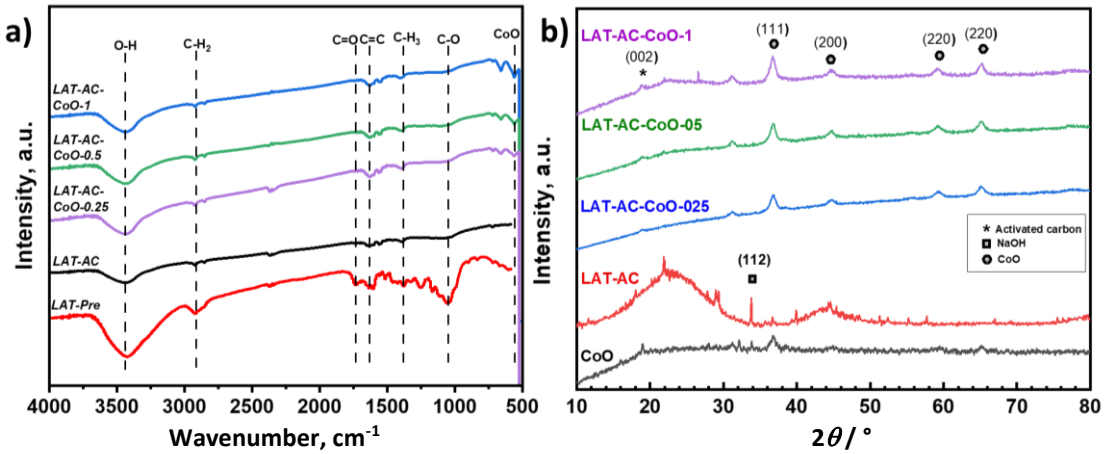

Figure 1. *(a) FTIR spectra of SB-based samples, including the sample before carbonization (LAT-Pre); (b) XRD results of activated carbon (LAT-AC), impregnated carbon (LAT-AC-CoO), and CoO samples*

In the XRD analysis in Figure 1(b), the peak from LAT-AC at 21.92° corresponds to the reflection (002), a graphite-like carbon structure. These (002) reflections indicate that the structure of AC is almost like graphite [21]. Besides that, a peak at 44.26° indicates a two-dimensional (101), usually owned by AC materials [22]. In addition, the peak from LAT-AC-CoO samples is in the 36.8 to 44.65° range with reflection due to the (111) plane of CoO, which proves the formation of only Co^{2+} ions, without the formation of Co^{3+}. It differs from the XRD result of CoO in Figure 1(b), which shows an amorphous nature, indicated by broad and uneven peaks. These peaks can be assigned to the amorphous structure, which formed due to the synthesis process using precipitation without further calcination prior to embedding in carbon LAT. The result indicates that during the hydrothermal process, no oxidation reaction of Co^{2+} to Co^{3+} is present [23].

The results of crystal size calculations for all samples are referred to in Table 2. Obviously, the carbon crystal size of 21.20 nm for LAT-AC is larger than for the other samples. After CoO impregnation, crystallite sizes became smaller (3.97 and 1.59 nm), which influences the specific capacitance of the material. Material with low crystallite size is beneficial in increasing specific capacitance [24].

Table 2. *Crystallite size of all SB-based samples and synthesized CoO*

Sample	2θ/°	FWHM	Compound	Crystallite size, nm
CoO	19.0	1.9201	CoO	0.08
LAT-AC	21.9	0.3816	Carbon	21.20
LAT-AC-CoO-025	22.3	2.0352	Carbon	3.97
	44.6	1.0176	CoO	8.44
LAT-AC-CoO-05	22.9	5.0880	Carbon	1.59
	44.6	1.0176	CoO	8.01
LAT-AC-CoO-1	18.9	0.7632	Carbon	10.55
	36.8	0.5732	CoO	14.62

After the pre-carbonization and calcination process, the carbon structure showed similarity, as indicated by the yellow peaks in the Raman spectra shown in Figure 2. After the addition of Co, there is evidence of the rearrangement in the carbon structure towards a more disordered state, as

observed by the increase in the D band intensity and I_D/I_G ratio. This rise in the D band and I_D/I_G ratio signifies increased structural defects or disorder within the carbon matrix.

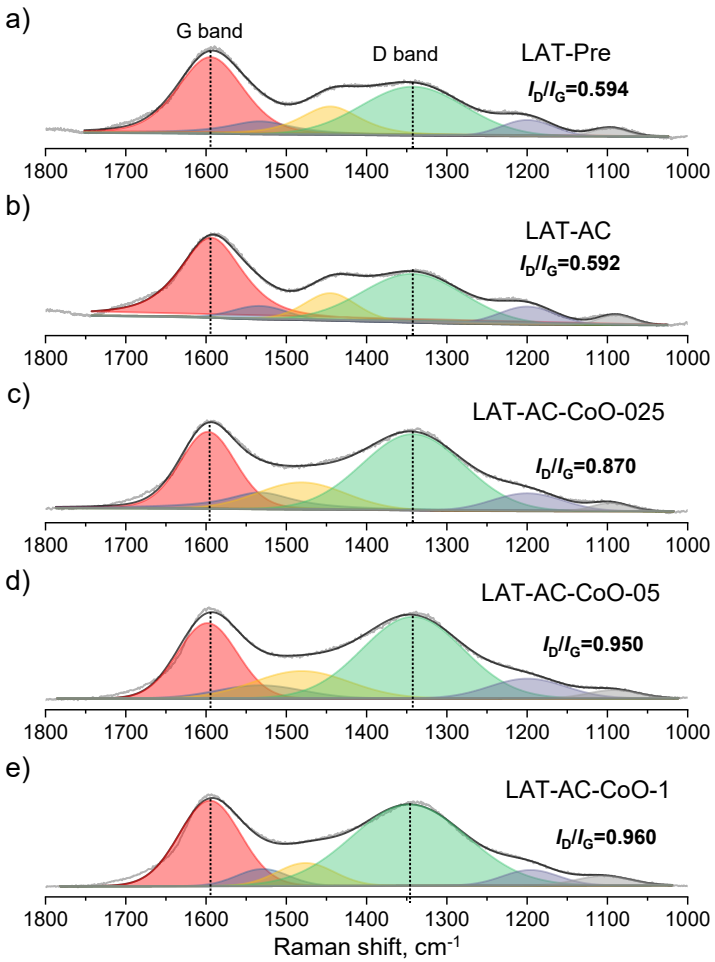

Figure 2. *Raman analysis of (a) LAT-Pre, (b) LAT-AC, (c) LAT-AC-CoO-025, (d) LAT-AC-CoO-05, (e) LAT-AC-CoO-1 samples*

As the Co content increases, the yellow peak gradually decreases, which suggests the vibrational mode's transformation in the carbon structure, such as changes in bonding due to doping or incorporation of cobalt. This decline indicates that higher Co content reduces ordered carbon regions, pointing to a more pronounced disruption or alteration in the carbon framework [25].

SEM analysis of each SB-based sample is shown in Figure 3. Figure 3(a) of the AC sample demonstrates that pores are formed uniformly after activation. These results are similar to previous studies on using SB for activated carbon preparation [26,27]. Next, Figures 3(b) and (c) of CoO-impregnated samples show small particles attached to the pore surfaces. These tiny particles are CoO that stick to the surface of AC after the impregnation process. Adding more CoO ratios will cover some sides of the pores that have already been opened, as can be seen in the SEM image in Figure 3(d).

From the results of the EDX analysis shown in Table 3, the components contained in LAT-AC are mostly C, which is 98.8 wt.%, and Na, which is 1.2 wt.%. For AC samples impregnated with CoO at different ratios, it was found that there are C and O components that are commonly owned by AC. In CoO-impregnated samples with the smallest ratio of 0.25, the CoO component was not detected in the EDX results. The result contradicted the FTIR result. We believe the CoO is placed within the pores and shown as small particles in the SEM images. However, EDX could not detect the content of CoO due to its tiny amount. The EDX images of all SB-based samples are shown in Figure 4.

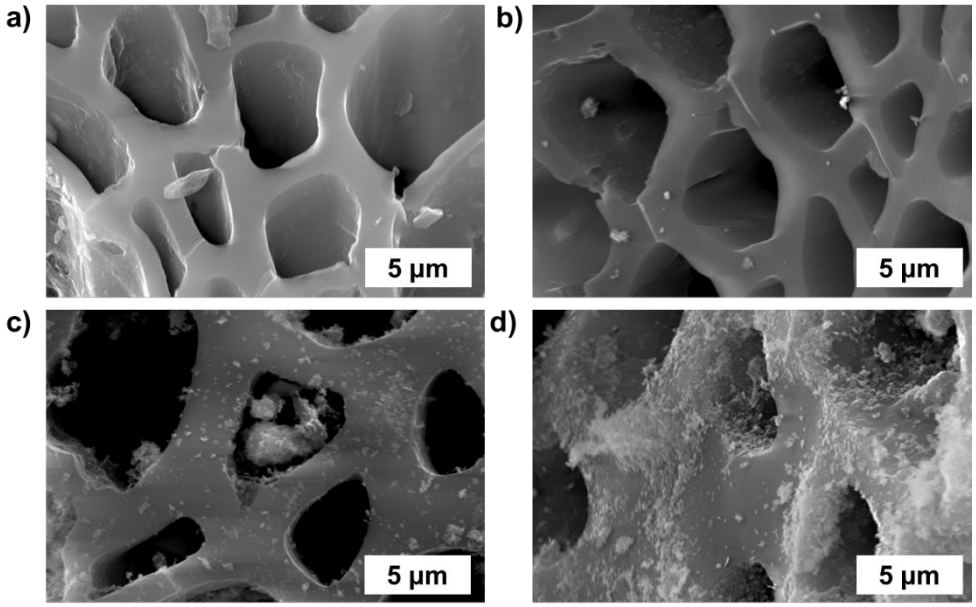

Figure 3. *SEM images of (a) LAT-AC, (b) LAT-AC-CoO-025, (c) LAT-AC-CoO-05, and (d) LAT-AC-CoO-1 samples*

Table 3. *Chemical composition of AC and AC impregnated by CoO samples obtained by EDX analysis*

Component	LAT-AC	LAT-AC-CoO-025	LAT-AC-CoO-05	LAT-AC-CoO-1
	Content, wt.%			
C	98.79	76.20	96.56	70.07
O	-	23.80	-	12.40
CoO	-	-	2.79	17.53
Na	1.21	-	0.65	-
Total	100.00	100.00	100.00	100.00

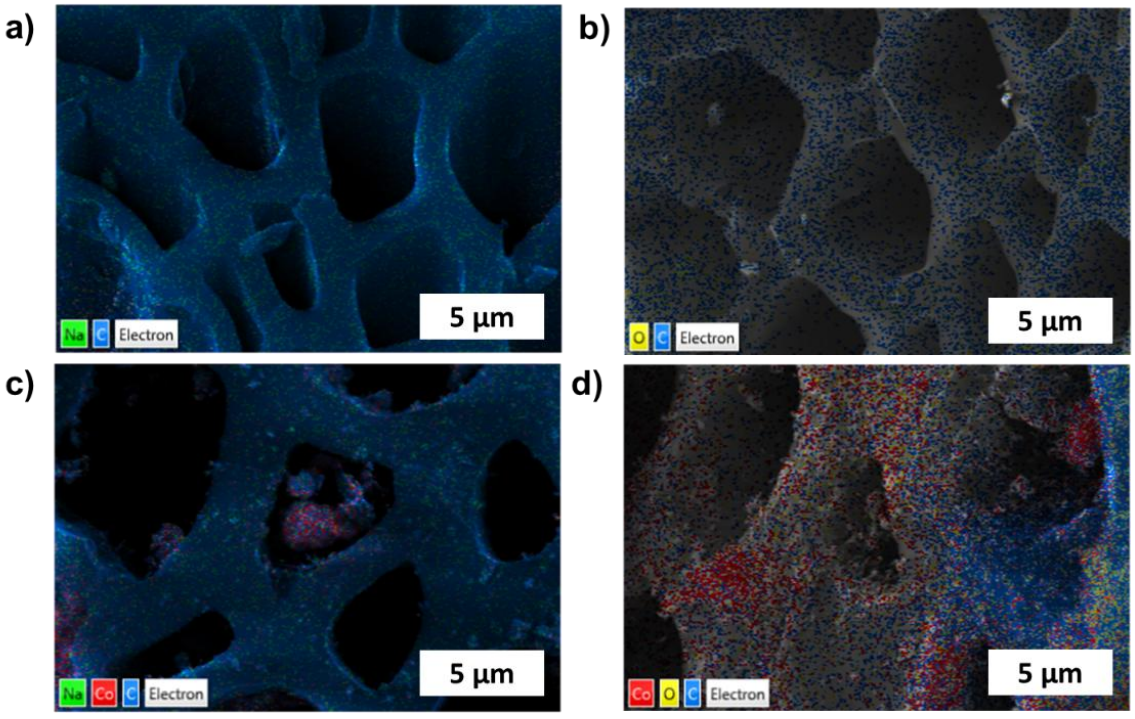

Figure 4. *EDX images of (a) LAT-AC (b) LAT-AC-CoO-025 (c) LAT-AC-CoO-05 (d) LAT-AC-CoO-1 samples*

The other two samples impregnated with CoO showed an even distribution of CoO. The presence of Na element (<1.2 %) originates probably from NaOH during activation. The opening of pores during activation makes Na enter and be trapped in the pore cavity. It seems that during the sample washing

process, Na is trapped and stays in AC pores. Based on the results of the SEM-EDX, it can be concluded that adding CoO to AC will affect the pore structure that has been formed and close ion access, affecting the performance of AC/CoO material as a supercapacitor electrode.

Figure 5 presents cyclic voltammograms (CVs) of each SB-based sample. CVs were performed within the potential window of -0.3 to 0.7 V *vs*. Ag/AgCl at various scan rates of 5 - 100 mV/s. The results in Figure 5a indicate that the CV curves from the LAT-Pre sample are still far from the EDLC mechanism. Next, the CV shapes of the LAT-AC sample shown in Figure 5b are almost like the EDLC mechanism, meaning no charge transfer occurs on the electrode-electrolyte surface during the charge-discharge process. The mechanism that occurs in EDLC storage involves the process of adsorption or desorption of ions from the electrolyte through an electrical double-layer structure on AC electrodes [28]. For LAT-AC samples impregnated with CoO, the CV curves in Figures 5c to 5e changed from square to irregular due to redox reactions between CoO and ions in the electrolyte. This characteristic corresponds to the mechanism of pseudocapacitors that can store charge through faradaic and EDLC surfaces at the same time [29].

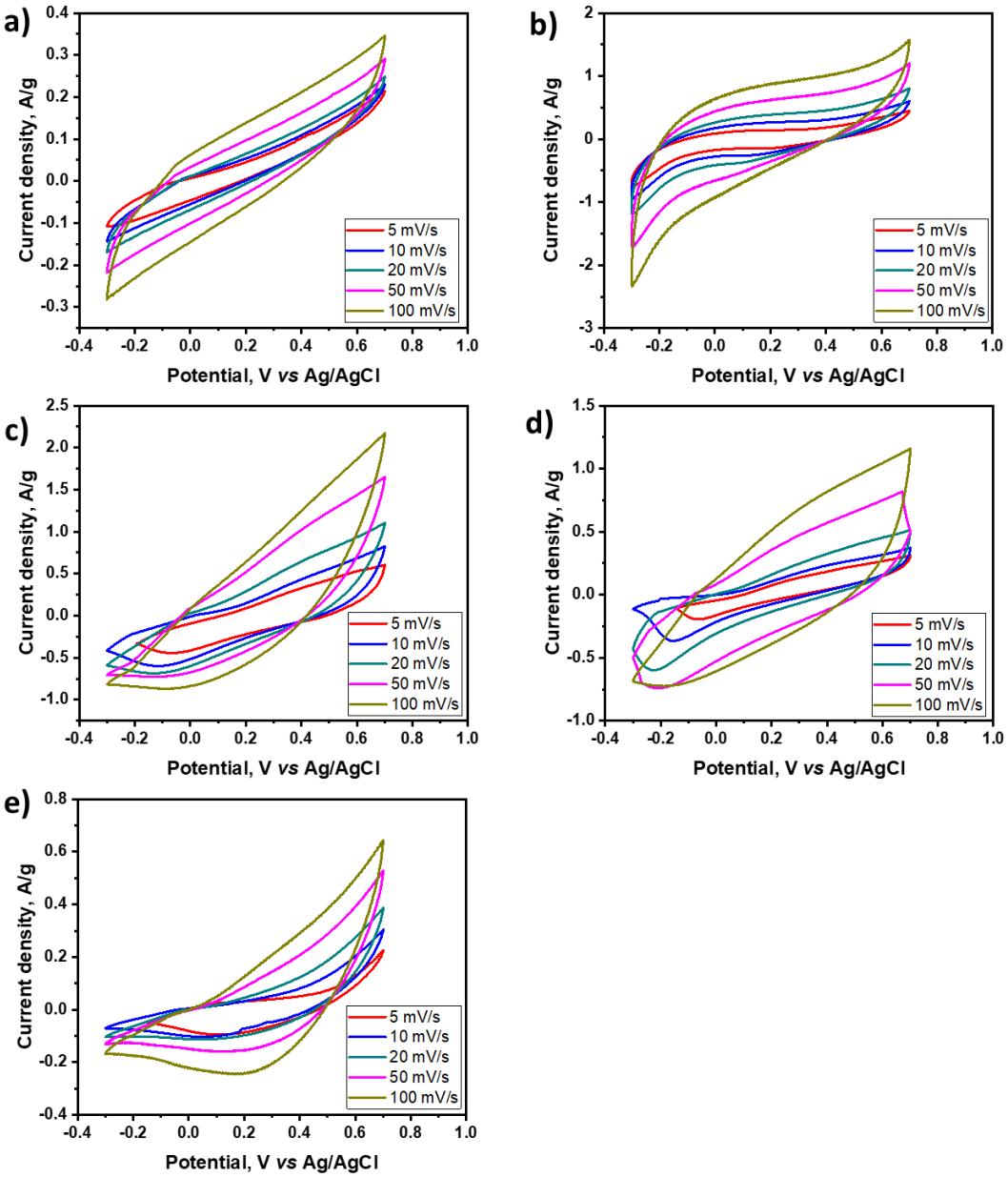

Figure 5. *CV curves at different potential scan rates of (a) LAT-Pre (b) LAT-AC (c) LAT-AC-025 (d) LAT-AC-CoO-05 and (e) LAT-AC-CoO1 electrodes*

Figure 6 shows the results of complete galvanostatic charging-discharging (GCD) tests for all SB-based samples at various current densities of 0.05 - 0.2 A/g. Briefly, the GCD curves of all samples show a triangle form that shows charge and discharge cycles. However, the graph of the GCD displayed forms a less-than-perfect triangle due to curvatures due to long charge and discharge time. The curvature formed in this GCD test is probably due to a reaction in AC impregnated with CoO and electrolyte ions, making the triangle area more expansive and the discharge time longer [30].

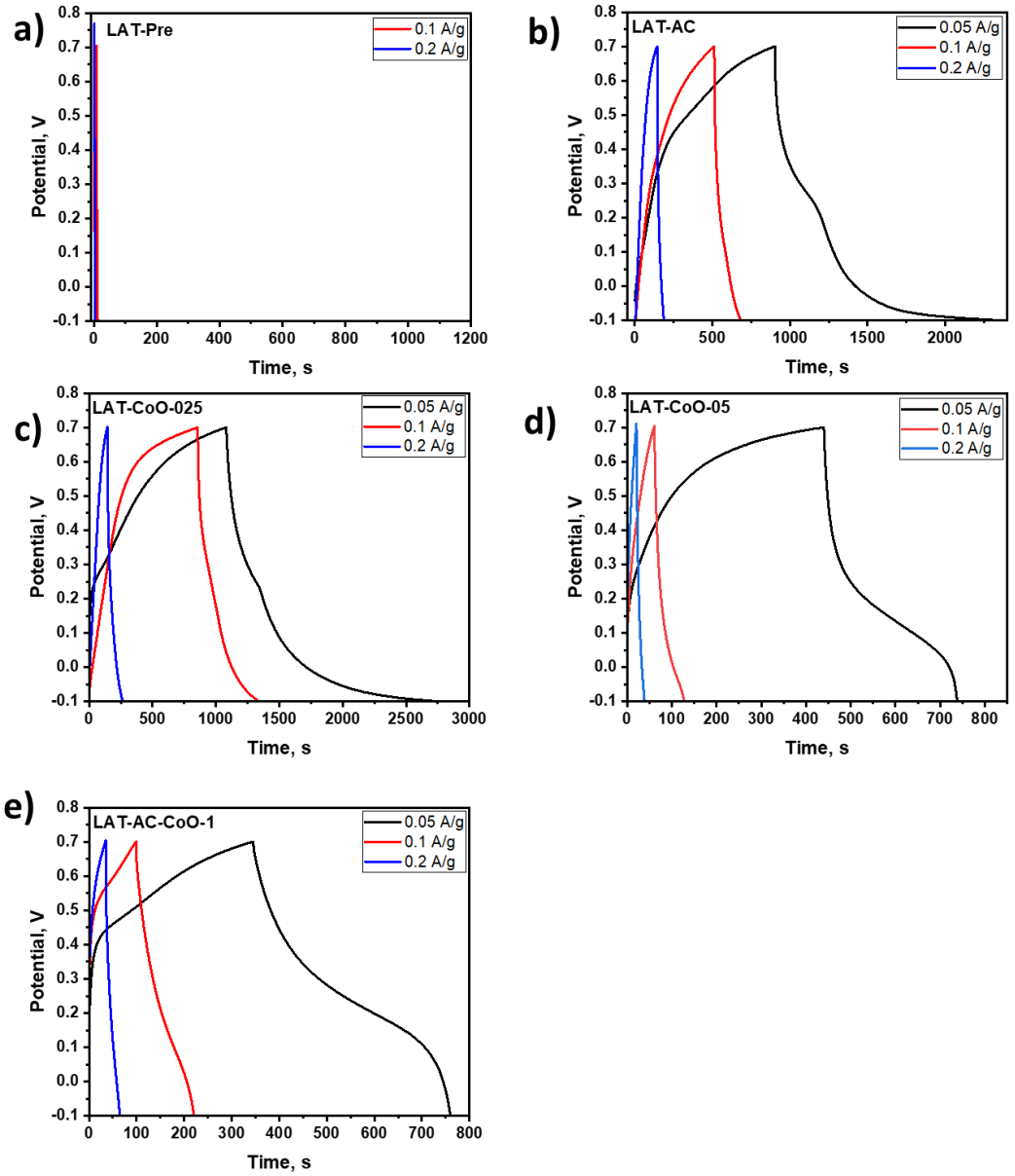

Figure 6. *GCD curves of (a) LAT-Pre, (b) LAT-AC, (c) LAT-AC-025, (d) LAT-AC-CoO-05 and (e) LAT-AC-CoO-1 electrode*

According to Figure 6(a), the readings for LAT-Pre samples can only be done at current densities of 0.1 A/g and 0.2 A/g, suggesting this material's very low storing charge ability. A minimal specific capacitance value of 0.77 F/g was obtained at the current density of 0.1 A/g. However, the GCD curves for the AC sample presented in Figure 7(b) showed a certain possibility of storing charge. After the activation process, the specific capacitance of LAT-AC increased to 89.53 F/g at a current density of 0.05 A/g. This value indicates that the process of opening pores has been carried out successfully to increase the specific capacitance of the material. The most considerable specific capacitance value of 102.04 F/g was obtained after the impregnation of AC with CoO in the ratio of

1:0.25. It is obvious that adding an excess of metal oxide cannot additionally increase specific capacitance. However, it can disrupt the redox process, limiting ion diffusion and reducing the capacitance [31]. While CoO has a high theoretical specific capacitance due to its pseudocapacitive properties, an excess amount can lead to inefficient utilization of its pseudocapacitive behavior. This inefficiency arises because only the surface of CoO is involved in fast redox reactions, and the bulk may remain electrochemically inactive if not properly distributed [32].

The complete results of specific capacitance calculations from GCD tests for all SB-based samples are presented in Table 4.

Table 4. *Specific capacitance values of SB-based samples obtained by GCD tests*

Sample	Current density, A/g	Specific capacitance, F/g
LAT-Pre	0.10	0.77
	0.20	0.50
LAT-AC	0.05	89.53
	0.10	20.93
	0.20	13.50
LAT-AC-CoO-025	0.05	102.04
	0.10	57.71
	0.20	28.30
LAT-AC-CoO-05	0.05	18.79
	0.10	8.42
	0.20	5.20
LAT-AC-CoO-1	0.05	25.99
	0.10	15.41
	0.20	7.70

The comparison of CVs at 5 mV/s and GCD results at 0.05 A/g for various samples is presented in Figure 7. Figure 7(a) shows that the highest current values are obtained for the AC/CoO-0.25 sample, suggesting the highest capacitances. The same is observed in Figure 7(b), which clearly demonstrates that LAT-AC impregnated with CoO in a smaller ratio (LAT-AC-0.25) shows a larger triangular area than all other samples. This larger triangular area means an increase in the specific capacitance value of the sample.

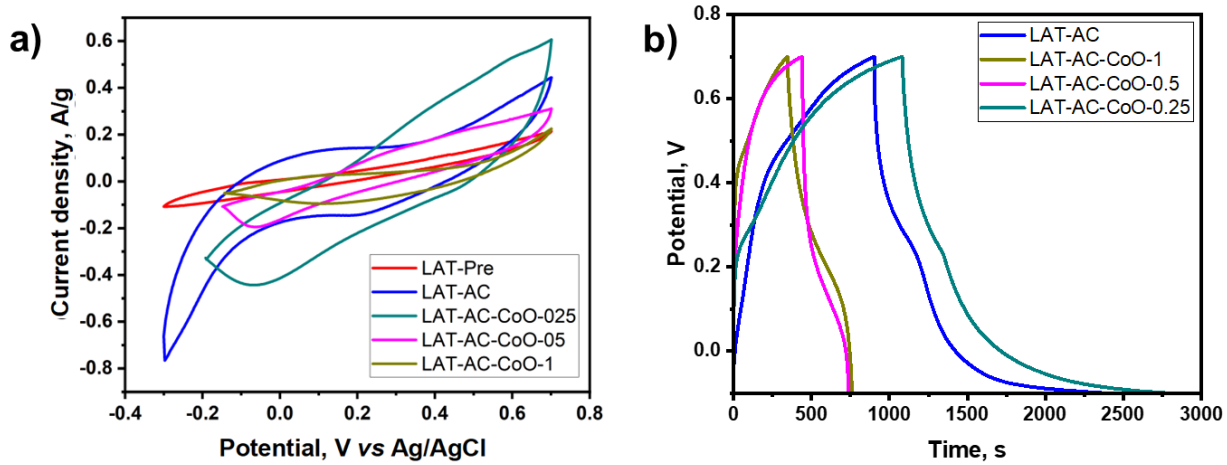

Figure 7. *Comparison of (a) CV curves at 5 mV/s and (b) GCD curves at 0.05 A/g for all SB-based samples*

Conclusions

Electrochemical results in this study showed that the specific capacitance of SB-based activated carbon impregnated with CoO is smaller than that of previous studies that used SB as a basis for activated carbon synthesis. However, this study has proven that SB can generally be used as a base

for manufacturing activated carbon, and the addition of CoO can be successfully carried out. These are evidenced by a Co-O functional group from the FTIR test and the appearance of a peak due to CoO from the XRD test. From the CV and GCD test results, it can be concluded that adding a small amount of CoO (LAT-AC-CoO-025 sample) can improve the electrochemical performance of the corresponding electrode compared to other electrodes. GCD results showed that for this electrode, the largest specific capacitance of 102.04 F/g at 0.05 A/g is obtained, compared to the activated carbon (LAT-AC sample) that showed 80.53 F/g. Other CoO-impregnated SB-based AC electrodes (LAT-AC-CoO-0.5 and LAT-AC-CoO-1 samples) showed lower specific capacitance values due to less efficient utilization of sites within the material bulk.

Acknowledgements: *This study was supported by selective research grants of Universitas Pertamina under the UPERESEARCH program 2022, also from the collaboration research between Universitas Pertamina and the Research Center for Biomass and Bioproduct, National Research and Innovation Agency (BRIN). The authors are also grateful for the support from Research and Technology Innovation, PT Pertamina (Persero).*

References

[1] S. Koohi-Fayegh, M. A. Rosen, A review of energy storage types, applications and recent developments, *Journal of Energy Storage* **27** (2020) 101047. https://doi.org/10.1016/j.est.2019.101047

[2] H. Feng, H. Hu, H. Dong, Y. Xiao, Y. Cai, B. Lei, Y. Liu, M. Zheng, Hierarchical structured carbon derived from bagasse wastes: A simple and efficient synthesis route and its improved electrochemical properties for high-performance supercapacitors, *Journal of Power Sources* **302** (2016) 164-173. https://doi.org/10.1016/j.jpowsour.2015.10.063

[3] J. Castro-Gutiérrez, A. Celzard, V. Fierro, Energy Storage in Supercapacitors: Focus on Tannin-Derived Carbon Electrodes, *Frontiers in Materials* **7** (2020) 217. https://doi.org/10.3389/fmats.2020.00217

[4] D. A. G. Hegde, Activated carbon nanospheres derived from bio-waste materials for supercapacitor applications - a review, *RSC Advances* **5** (2015) 88339-88352. https://doi.org/10.1039/C5RA19392C

[5] O. Ioannidou, A. Zabaniotou, Agricultural residues as precursors for activated carbon production—A review, *Renewable and Sustainable Energy Reviews* **11** (2007) 1966-2005. https://doi.org/10.1016/j.rser.2006.03.013

[6] Z. Tan, J. Yang, Y. Liang, M. Zheng, H. Hu, H. Dong, Y. Liu, Y. Xiao, The changing structure by component: Biomass-based porous carbon for high-performance supercapacitors, *Journal of Colloid and Interface Science* **585** (2021) 778-786. https://doi.org/10.1016/j.jcis.2020.10.058

[7] J.. Sun, X. Sun, H. Zhao, R. Sun, Isolation and characterization of cellulose from sugarcane bagasse, *Polymer Degradation and Stability* **84** (2004) 331-339. https://doi.org/10.1016/j.polymdegradstab.2004.02.008

[8] Lichchhavi, A. Kanwade, P. M. Shirage, A review on synergy of transition metal oxide nanostructured materials: Effective and coherent choice for supercapacitor electrodes, *Journal of Energy Storage* **55** (2022) 105692. https://doi.org/10.1016/j.est.2022.105692

[9] M. Girirajan, A. K. Bojarajan, I. N. Pulidindi, K. N. Hui, S. Sangaraju, An insight into the nanoarchitecture of electrode materials on the performance of supercapacitors, *Coordination Chemistry Reviews* **518** (2024) 216080. https://doi.org/https://doi.org/10.1016/j.ccr.2024.216080

[10] H. W. Park, K. C. Roh, Recent advances in and perspectives on pseudocapacitive materials for Supercapacitors, *Journal of Power Sources* **557** (2023) 232558. https://doi.org/https://doi.org/10.1016/j.jpowsour.2022.232558
[11] Annu, S.-S. Park, M. N. Alam, M. Yewale, D. K. Shin, Unraveling the Electrochemical Insights of Cobalt Oxide/Conducting Polymer Hybrid Materials for Supercapacitor, Battery, and Supercapattery Applications, *Polymers (Basel)* **16** (2024) 2907. https://doi.org/10.3390/polym16202907
[12] A. P. Khedulkar, V. D. Dang, A. Thamilselvan, R. Doong, B. Pandit, Sustainable high-energy supercapacitors: Metal oxide-agricultural waste biochar composites paving the way for a greener future, *Journal of Energy Storage* **77** (2024) 109723. https://doi.org/https://doi.org/10.1016/j.est.2023.109723
[13] Y. Wang, J. Guo, T. Wang, J. Shao, D. Wang, Y.-W. Yang, Mesoporous Transition Metal Oxides for Supercapacitors, *Nanomaterials* **5** (2015) 1667-1689. https://doi.org/10.3390/nano5041667
[14] R. F. Susanti, R. G. R. Wiratmadja, H. Kristianto, A. A. Arie, A. Nugroho, Synthesis of high surface area activated carbon derived from cocoa pods husk by hydrothermal carbonization and chemical activation using zinc chloride as activating agent, *Materials Today: Proceedings* **63** (2022) S55-S60. https://doi.org/10.1016/j.matpr.2022.01.042
[15] R. E. Haraki, A. A. Arie, R. F. Susanti, H. S. Oktaviano, A. Nugroho, Synthesis and Electrochemical Properties of ZnO/Activated Carbon from Vetiver Distillation Waste, *Engineering Chemistry* **2** (2023) 35-41. https://doi.org/10.4028/p-1z7h01
[16] H. Yang, R. Yan, H. Chen, D. H. Lee, C. Zheng, Characteristics of hemicellulose, cellulose and lignin pyrolysis, *Fuel* **86** (2007) 1781-1788. https://doi.org/10.1016/j.fuel.2006.12.013
[17] M. Dwiyaniti, A.. Elang Barruna, R. Muhamad Naufal, I. Subiyanto, R. Setiabudy, C. Hudaya, Extremely high surface area of activated carbon originated from sugarcane bagasse, *IOP Conference Series: Materials Science and Engineering* **909** (2020) 012018. https://doi.org/10.1088/1757-899X/909/1/012018
[18] A. F. Hassan, A. M. Youssef, Preparation and characterization of microporous NaOH-activated carbons from hydrofluoric acid leached rice husk and its application for lead(II) adsorption, *Carbon Letters* **15** (2014) 57-66. https://doi.org/10.5714/CL.2014.15.1.057
[19] X. Li, Y. Jiang, P. Wang, Y. Mo, W. Lai, Z. Li, R. Yu, Y. Du, X. Zhang, Y. Chen, Effect of the oxygen functional groups of activated carbon on its electrochemical performance for supercapacitors, *New Carbon Materials* **35** (2020) 232-243. https://doi.org/10.1016/S1872-5805(20)60487-5
[20] M. Rahimi-Nasrabadi, H. R. Naderi, M. S. Karimi, F. Ahmadi, S. M. Pourmortazavi, Cobalt carbonate and cobalt oxide nanoparticles synthesis, characterization and supercapacitive evaluation, *Journal of Materials Science: Materials in Electronics* **28** (2017) 1877-1888. https://doi.org/10.1007/s10854-016-5739-z
[21] S. Sarkar, A. Arya, U. K. Gaur, A. Gaur, Investigations on porous carbon derived from sugarcane bagasse as an electrode material for supercapacitors, *Biomass and Bioenergy* **142** (2020) 105730. https://doi.org/10.1016/j.biombioe.2020.105730
[22] R. Azargohar, A. K. Dalai, Biochar As a Precursor of Activated Carbon, *Applied Biochemistry and Biotechnology* **131** (2006) 762-773. https://doi.org/10.1385/ABAB:131:1:762
[23] D. J. Tarimo, K. O. Oyedotun, A. A. Mirghni, B. Mutuma, N. F. Sylla, P. Murovhi, N. Manyala, Enhanced electrochemical performance of supercapattery derived from sulphur-reduced graphene oxide/cobalt oxide composite and activated carbon from peanut shells, *International Journal of Hydrogen Energy* **45** (2020) 33059-33075. https://doi.org/10.1016/j.ijhydene.2020.09.142

[24] S. Xiong, Y. He, X. Zhang, B. Wu, J. Chu, X. Wang, R. Zhang, M. Gong, Z. Li, Z. Chen, Hydrothermal synthesis of high specific capacitance electrode material using porous bagasse biomass carbon hosting MnO2 nanospheres, *Biomass Conversion and Biorefinery* **11** (2021) 1325-1334. https://doi.org/10.1007/s13399-019-00525-y

[25] A. C. Ferrari, J. Robertson, Interpretation of Raman spectra of disordered and amorphous carbon, *Physical Review B* **61** (2000) 14095-14107. https://doi.org/10.1103/PhysRevB.61.14095

[26] E. Taer, Iwantono, S. T. Manik, R. Taslim, D. Dahlan, M. Deraman, Preparation of Activated Carbon Monolith Electrodes from Sugarcane Bagasse by Physical and Physical-Chemical Activation Process for Supercapacitor Application, *Advanced Materials Research* **896** (2014) 179-182. https://doi.org/10.4028/www.scientific.net/AMR.896.179

[27] T. Adinaveen, L. J. Kennedy, J. J. Vijaya, G. Sekaran, Studies on structural, morphological, electrical and electrochemical properties of activated carbon prepared from sugarcane bagasse, *Journal of Industrial and Engineering Chemistry* **19** (2013) 1470-1476. https://doi.org/10.1016/j.jiec.2013.01.010

[28] Y. Wang, L. Zhang, H. Hou, W. Xu, G. Duan, S. He, K. Liu, S. Jiang, Recent progress in carbon-based materials for supercapacitor electrodes: a review, *Journal of Materials Science* **56** (2020) 173-200. https://doi.org/10.1007/S10853-020-05157-6

[29] N. R. Chodankar, H. D. Pham, A. K. Nanjundan, J. F. S. Fernando, K. Jayaramulu, D. Golberg, Y. Han, D. P. Dubal, True Meaning of Pseudocapacitors and Their Performance Metrics: Asymmetric versus Hybrid Supercapacitors, *Small* **16** (2020) 2002806. https://doi.org/10.1002/smll.202002806

[30] V. Sannasi, K. Subbian, Influence of Moringa oleifera gum on two polymorphs synthesis of MnO_2 and evaluation of the pseudo-capacitance activity, *Journal of Materials Science: Materials in Electronics* **31** (2020) 17120-17132. https://doi.org/10.1007/s10854-020-04272-z

[31] A. Pradiprao Khedulkar, V. Dien Dang, B. Pandit, T. Ai Ngoc Bui, H. Linh Tran, R. Doong, Flower-like nickel hydroxide@tea leaf-derived biochar composite for high-performance supercapacitor application, *Journal of Colloid and Interface Science* **623** (2022) 845-855. https://doi.org/10.1016/j.jcis.2022.04.178

[32] J. Wang, S. Dong, B. Ding, Y. Wang, X. Hao, H. Dou, Y. Xia, X. Zhang, Pseudocapacitive materials for electrochemical capacitors: from rational synthesis to capacitance optimization, *National Science Review* **4** (2017) 71-90. https://doi.org/10.1093/nsr/nww072